Exploring high-energy doubly excited states of NH by dissociative recombination of NH^+

2014 J. Phys. B: At. Mol. Opt. Phys. 47 035201

(http://iopscience.iop.org/0953-4075/47/3/035201)

IOP Publishing Journal of Physics B: Atomic, Molecular and Optical Physics

J. Phys. B: At. Mol. Opt. Phys. **47** (2014) 035201 (6pp) doi:10.1088/0953-4075/47/3/035201

Exploring high-energy doubly excited states of NH by dissociative recombination of NH^+

B Yang[1,2,3,7], O Novotný[2,4], C Krantz[2], H Buhr[5], M Mendes[2], C Nordhorn[2], W D Geppert[6], M Grieser[2], R Repnow[2], M Berg[2], D Bing[2], C Domesle[2], F Grussie[2], D Wolf Savin[4], D Schwalm[2,5], X Cai[1] and A Wolf[2]

[1] Institute of Modern Physics, Chinese Academy of Sciences, Lanzhou 730000, People's Republic of China
[2] Max Planck Institute for Nuclear Physics, D-69117 Heidelberg, Germany
[3] University of Chinese Academy of Sciences, Beijing 100049, People's Republic of China
[4] Columbia Astrophysics Laboratory, Columbia University, New York, NY 10027, USA
[5] Department of Particle Physics, Weizmann Institute of Science, Rehovot 76100, Israel
[6] Department of Physics, Stockholm University, AlbaNova, SE-106 91 Stockholm, Sweden

E-mail: yangbian@impcas.ac.cn and A.Wolf@mpi-hd.mpg.de

Received 22 August 2013, revised 29 November 2013
Accepted for publication 9 December 2013
Published 10 January 2014

Abstract

We have investigated electron capture by NH^+ resulting in dissociative recombination (DR). The impact energies studied of ∼4–12 eV extend over the range below the two lowest predicted NH^+ dissociative states in the Franck–Condon (FC) region of the ion. Our focus has been on the final state populations of the resulting N and H atoms. The neutral DR fragments are detected downstream of a merged electron and ion beam interaction zone in the TSR storage ring, which is located at the Max Planck Institute for Nuclear Physics in Heidelberg, Germany. Transverse fragment distances were measured on a recently developed high count-rate imaging detector. The distance distributions enabled a detailed tracking of the final state populations as a function of the electron collision energy. These can be correlated with doubly excited neutral states in the FC region of the ion. At low electron energy of ∼5 eV, the atomic product final levels are nitrogen Rydberg states together with ground-state hydrogen. In a small electron energy interval near 7 eV, a significant part of the final state population forms hydrogen Rydberg atoms with nitrogen atoms in the first excited (^{2}D) term, showing the effect of Rydberg doubly excited states below the predicted $2\,^2\Pi$ ionic potential. The distance distributions above ∼10 eV are compatible with nitrogen Rydberg states correlating to the doubly excited Rydberg state manifold below the ionic $2\,^4\Sigma^-$ level.

Keywords: dissociative recombination, doubly excited molecular states, molecular collisions

(Some figures may appear in colour only in the online journal)

When two electrons in a molecule are transferred to orbitals not populated in the ground state, a doubly excited state is created. Such states play a key role [1] in the collisional or radiative excitation of molecules at energies high above the ionization limit and can result in dissociation into energetic neutral fragments. On a femtosecond timescale, this fragmentation competes with the autoionization of the doubly excited state into ions and photoelectrons. While autoionization reflects the electron correlations within the molecule, the fragment properties are determined by the molecular dynamics in the dissociation process. Often the products from the fragmentation of doubly excited molecules are themselves electronically excited. In the fragmentation process, the rapid variation of the internuclear distances can distribute the dissociating molecular quantum state over different potential

[7] Author to whom any correspondence should be addressed.

surfaces and has a large influence on the product state populations.

Because of the fundamental interest in these processes, photoionization studies of electronic and nuclear dynamics via doubly excited states are being performed at synchrotron light sources [2, 3] and by intense laser pulses [4, 5]. Doubly excited molecular states are also created when a molecular ion is excited by a colliding electron which is simultaneously captured. This initial step in the dissociative recombination (DR) [6] process is followed by dissociation into neutral fragments. Depending on the properties of the doubly excited potential surfaces, the products can carry both kinetic energy (E_k) and internal excitation. Experimentally, the DR process can be studied in ion storage rings using electrons with a well-defined collision energy E [7]. Additionally, the kinetic energy release (KER) E_k can be obtained by measuring the relative velocities of the fragments [8]. In combination, these methods enable sensitive investigations of doubly excited molecular states and their fragmentation.

In this paper, we describe recent advances in DR studies of doubly excited states in a multi-electron diatomic molecule. Measurements were made using a merged electron and ion beams geometry in an ion storage ring in combination with a high-efficiency position sensitive detector for the neutral fragments [8]. With this configuration, we were able to observe the relative velocity distribution of the fragments and track how this distribution changed as the electron impact energy was varied. We use these data to characterize the dissociating doubly excited states of the neutral molecule formed in the DR process. As our results below demonstrate, the KER in DR as a function of the collision energy offers a powerful method for probing the doubly excited neutral states in the Franck–Condon (FC) region of a molecular ion, as well as their fragmentation pathways. In the present work, we consider neutral fragmentation pathways of those doubly excited levels which dissociate directly, rather than through an intermediate neutral bound resonance. For DR, this implies collision energies above the rotational and vibrational excitation energies of the ion as well as above its bound electronically excited states.

Here we report results on the nitrogen hydride radical cation NH^+, for which the DR reaction proceeds as

$$NH^+ + e(E) \rightarrow NH^{**} \rightarrow \left\{ \begin{matrix} N + H \\ N^* + H \\ N + H^* \\ N^* + H^* \end{matrix} \right\} + E_k. \qquad (1)$$

NH^{**} denotes a doubly excited state formed by capture of the free electron e, N^* and H^* are electronically excited atomic fragments and E_k is the KER. Figure 1 gives an overview of the calculated singly excited potential energy curves of the ion (NH^+) as well as some singly and doubly excited curves for the neutral (NH). For this schematic overview, graphical representations of calculated potential curves of NH^+ [9] and NH [10] were overlaid assuming the adiabatic ionization energy of NH as given in [9]. The energy accuracy in this scheme is estimated to be at the ± 0.1 eV level, sufficient for our considerations here. The internal energies of the associated atomic fragment states are also shown. The NH^+ ground state is assigned to the $X\,^2\Pi$ potential, while the lowest state of the $a\,^4\Sigma^-$ potential lies $\sim$0.04 eV above the ground state [11]. As discussed below, the ions used in the experiment are expected to be in their vibrational ground state with a remaining internal excitation of < 0.1 eV. This includes a possible population in the $a\,^4\Sigma^-$ state. The initial states involved in the DR reaction lie in the FC region, indicated in figure 1. Since the present work focuses on directly dissociating doubly excited states, we consider only impact energies above that needed to reach the highest bound potential curve of the ion, $C\,^2\Sigma^+$. This implies collision energies above $E = 4.2$ eV.

Doubly excited states occur when an outer electron is bound to an excited state of the ion. Hence, their energies lie below the corresponding ionic potential energy curve by an amount that reflects the binding energy. Doubly excited states that lie at small energies of <1 eV below an ionic curve we denote as high-Rydberg doubly excited states, while for higher binding energies of the outer electron, we denote them as low-Rydberg or valence-type doubly excited states. Based on the calculations shown in figure 1, the doubly excited states in the FC region for the energy range considered are expected to be associated mainly with the ionic states $2\,^2\Pi$ and $2\,^4\Sigma^-$ and can be either of high-Rydberg or of low-Rydberg or valence character.

The experiment was carried out using the TSR storage ring [12] located at the Max Planck Institute for Nuclear Physics in Heidelberg, Germany. NH_2^- anions from a sputtering ion source were accelerated in a tandem accelerator and stripped on the high-voltage terminal to form NH^+ with a kinetic energy of $E_{ion} = 6.203$ MeV. This beam was injected into TSR using multi-turn injection and stored at this energy in a vacuum of $\sim 3 \times 10^{-11}$ mbar. After injection, the NH^+ ions were continuously phase-space cooled [13] using the velocity matched electron beams from the electron cooler [14] (equipped with a thermocathode) and the electron target [15–17] (equipped with a cryogenic photocathode electron source [18]). After 6 s of electron cooling, the parent ion NH^+ is expected to have radiatively de-excited to the vibrational ground levels of the $X\,^2\Pi$ or $a\,^4\Sigma^-$ electronic states. In fact, the natural lifetimes of states belonging to the bound excited $A\,^2\Sigma^-$, $B\,^2\Delta$ and $C\,^2\Sigma^+$ curves were found to be $< 1.2\ \mu$s [19], while the lifetimes of vibrationally excited states in $X\,^2\Pi$ and $a\,^4\Sigma^-$ are estimated (using the method of [20]) to be < 30 ms. Regarding pure rotational excitation, the lifetimes of the most populated levels at the $\sim$300 K ambient temperature of TSR are estimated to $\sim$1.6 s. Hence, the rotational distribution after the electron cooling period should be essentially thermalized and reflect the ambient temperature. Given the uncertainty of the population in a $^4\Sigma^-$ states, we estimate the internal excitation of the cooled NH^+ ions to be < 0.1 eV. The beam of the electron target is $\sim$1.1 m in effective length. It can not only cool the ion beam, but can also serve as the interaction medium for DR studies at well-defined collision energies. In the range of interest for this work, the energy resolution was < 0.03 eV and the collision energy was changed by setting the laboratory energy of the target electron beam between $\sim$293 and 342 eV. The electron density was in the range of $\sim 2 \times 10^6 \mathrm{cm}^{-3}$. Neutral fragments produced by DR continued ballistically along the

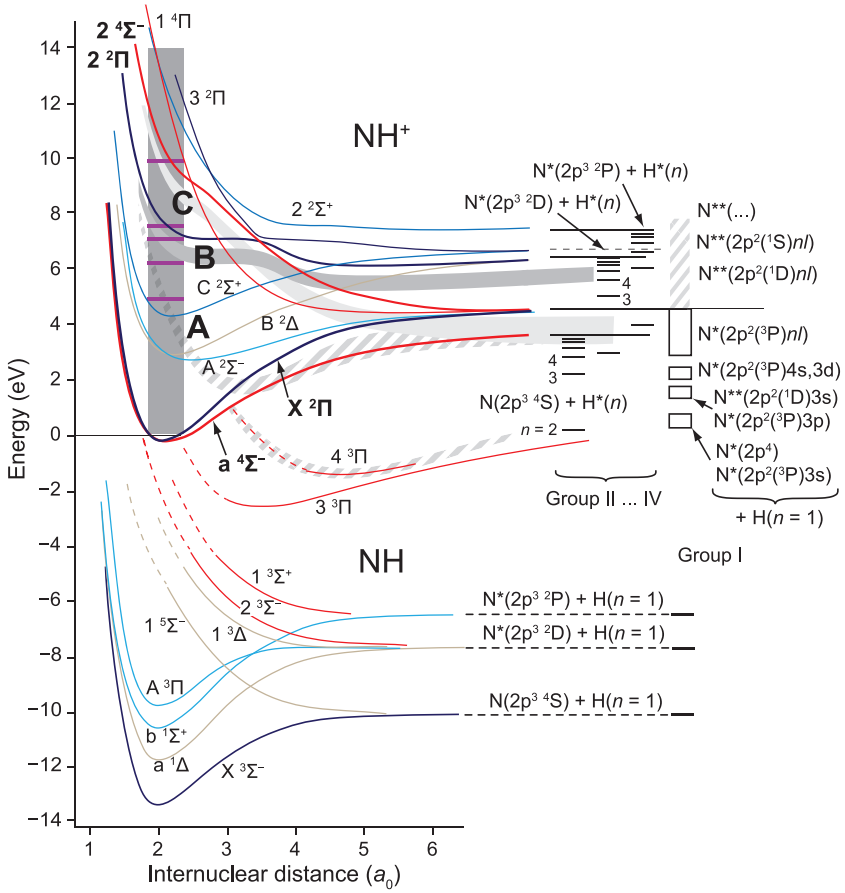

Figure 1. A schematic of calculated potential energy curves for NH^+ [9] and NH [10] together with the FC region (gray rectangle) and the possible final states of the N and H fragments for the DR of NH^+ (see text). Electron energies for which $P(d)$ distributions are presented in figure 2 are indicated by the horizontal marks in the FC region. The fragmentation pathways inferred from measured $P(d)$ distributions are schematically indicated by the bands labelled A (hatched), B (dark grey) and C (light grey). The dashed parts of some neutral potential curves indicate their estimated continuation as diabatic states through avoided crossings with higher curves.

beamline downstream of the electron target. The stored ion beam is deflected by one of the TSR dipole magnets, while the neutrals are recorded by dedicated detectors. Total count rates can be analysed to derive absolute recombination rate coefficients using a non-imaging surface barrier detector [21]. The imaging detector yields the transverse distance d between the N and H fragment atoms on an event by event basis. This distance is proportional to the relative velocity of the DR fragments projected onto the plane transverse to the interacting beams [22].

The KER E_k of the neutral fragments is given by

$$E_k = E + E_{k,0} + E_i(NH^+) - E_f(N) - E_f(H), \qquad (2)$$

where $E_{k,0}$ denotes the KER for DR from the ground state of the parent ions to ground-state neutral fragments for negligible electron energy ($E = 0$). The KER increases as either the electron collision energy E or the excitation energy $E_i(NH^+)$ of the parent ion increases. The KER decreases as either the excitation energies $E_f(N)$ or $E_f(H)$ of the products increases. In the present case $E_{k,0} = 10.07$ eV and, considering the relatively high value of E of interest in this work, we neglect $E_i(NH^+)$. The expected value of E_k can be calculated from the tabulated excitation energies [23] of $E_f(N)$ and $E_f(H)$. The energies of the various possible final levels are indicated in figure 1.

Table 1. Atomic product state groups for DR of NH^+ (see figure 1).

Group ID	Fragment H	Fragment N
I	$H(n = 1)$	N, N^*
II	$H^*(n \geqslant 2)$	$N(2p^3\ ^4S)$
III	$H^*(n \geqslant 2)$	$N^*(2p^3\ ^2D)$
IV	$H^*(n \geqslant 2)$	$N^*(2p^3\ ^2P)$

We order these final levels into four groups as given in table 1. The channel with ground-state or excited nitrogen (N, N^*) and with ground-state H is identified as group I. This includes the $N^*(2p^2(^3P)nl)$ Rydberg series but excludes other N levels above the first ionization limit, leading to $N^+(2p^2\ ^3P)$, as they are expected to autoionize on less than a ps timescale [24]. Channels with N in the three terms of the ground configuration and $H^*(n \geqslant 2)$ are identified as groups II, III and IV and include Rydberg hydrogen fragments together with ^4S, ^2D, and ^2P nitrogen, respectively. Levels with $H^*(n \geqslant 2)$ and N excited to higher configurations are outside the energy range considered.

In our experiment, E_k determines the distribution of transverse distances d measured between the two neutral products at the fragment imaging detector. We use the recently developed energy-sensitive multi-strip detector (EMU) [8],

which separately identifies the N and H fragments by their masses and, with a sensitive area of $100 \times 100\,\mathrm{mm}^2$, measures their positions with a resolution of 0.76 mm. Count rates up to $\sim 2 \times 10^3\ \mathrm{s}^{-1}$ can be achieved. The distance d can be readily calculated for two-body fragmentation given a fixed E_k, a fragmentation angle θ in the rest frame of the ion ($\theta = 0$ along the beam axis) and an event distance s from the detector. The transverse projected distance [22] is $d = s(ME_\mathrm{k}/\mu E_\mathrm{ion})^{1/2} \sin\theta$, where $M = 15$ u and $\mu = (14/15)$ u are the total and the reduced masses of NH in atomic mass units, respectively. Since the stored molecular ions are randomly oriented, the internuclear axes have no preferential direction. Moreover, low electronic angular momenta are typically involved in the DR process [6]. Thus, the fragmentation angles are generally distributed over a wide range and a distribution of transverse distances, $P(d)$, is observed even for a single value of E_k. A precise prediction of the angular distribution (essentially the angular dependence of the DR cross section) would require the knowledge of the angular quantum numbers for the individual doubly excited states involved. These are not available for the present case. However, for most cases, the distribution $P(d)$ can be expected to extend up to the largest distance, occurring when $\sin\theta = 1$. Moreover, nearly transverse values of θ ($\sin\theta \sim 1$) are favoured by their larger emission angle, which gives them a higher weight in $P(d)$. For most DR angular dependences, the maximum of $P(d)$ is expected [22] near $d = d_\mathrm{max}$ with

$$d_\mathrm{max} = L_< (ME_\mathrm{k}/\mu E_\mathrm{ion})^{1/2}, \qquad (3)$$

where $L_<$ denotes the smallest distance to the detector for the interaction region (for the present results, $L_< = 8.86$ m). Since in the present interpretation of the experimental results, we do not aim at a precise quantitative comparison with predictions, we consider the value of d_max as indicative for the respective KER.

At the high count rates which could be handled by the EMU system, we have been able to acquire fragment distance distributions $P(d)$ for a large number of different collision energies covering all the energy range from $E = 0$ up to 11.7 eV. At energies $E < 4.2$ eV, we found that the product channels $\mathrm{H}(n = 1) + \mathrm{N}(2\mathrm{s}^2 2\mathrm{p}^3(^2\mathrm{D},^2\mathrm{P}))$, $\mathrm{H}(n = 2) + \mathrm{N}(2\mathrm{s}^2 2\mathrm{p}^3(^4\mathrm{S}))$ and $\mathrm{H}(n = 1) + \mathrm{N}(2\mathrm{s}^2 2\mathrm{p}^2 3\mathrm{s}(^4\mathrm{P},^2\mathrm{P}))$ sequentially became important as the electron collision energy E increased. At these low energies, the DR cross section also showed sharp resonant structure related to bound neutral doubly excited levels. These results, requiring specialized analysis methods, will be presented in forthcoming publications [21, 25]. In contrast, over the energy range $E = 4.2$–11.7 eV where DR proceeds directly via dissociating doubly excited states, we find that the merged beams recombination rate coefficient increases smoothly from $1.7(2) \times 10^{-9}\ \mathrm{cm}^3\ \mathrm{s}^{-1}$ at 5 eV up to a maximum of $7.8(4) \times 10^{-9}\ \mathrm{cm}^3\ \mathrm{s}^{-1}$ at 10.1 eV, followed by a slight decrease for higher values. (Here and throughout the number in parenthesis represents the 1σ statistical uncertainty in the last significant digit given.) These preliminary rate coefficients are derived from the measured integral count rates, details of which will be presented in [21].

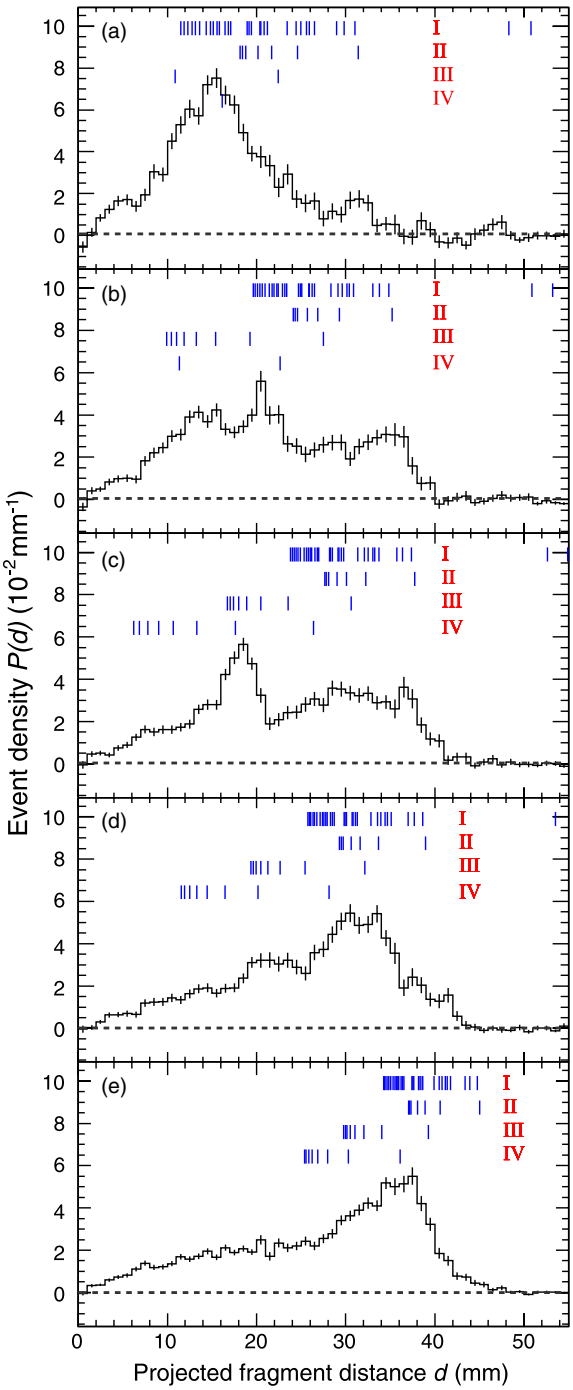

Figure 2. Normalized projected fragment distance distribution $P(d)$ acquired for DR of NH^+ at the selected collision energies E of 5.0 eV (a), 6.2 eV (b), 7.1 eV (c), 7.6 eV (d) and 10.1 eV (e). The histogram shows the measured data with a bin width in d of 1 mm and vertical error bars representing the 1σ statistical uncertainties. The blue vertical marks give the values of d_max calculated from equations (2) and (3) for the accessible final levels (figure 1; group labels from table 1). The distributions $P(d)$ are normalized to unit area. The preliminary merged beams rate coefficients (in $10^{-9}\ \mathrm{cm}^3\ \mathrm{s}^{-1}$) are 1.7(2), 3.2(2), 4.4(4), 4.2(4) and 7.8(4) for panels (a)–(e), respectively.

The dependence of $P(d)$ on E is illustrated by selected plots in figure 2. Over the range from $E = 4.2$ to 5.0 eV, the shape of $P(d)$ is similar to figure 2(a). We have calculated the

expected positions of d_{max} for the various possible final levels, given in figure 1 and table 1; these positions are marked in figure 2 for the respective values of E. Using equations (2) and (3), one can readily see that smaller values of d_{max} correspond to higher excitation levels in the atomic products. With these as a guide, we find that DR is dominated in this energy range by dissociation into group I, high nitrogen Rydberg levels and ground-state hydrogen. These values of E lie above all the bound NH^+ curves in the FC region, but they all still lie much below the higher $2\,^2\Pi$ and $2\,^4\Sigma^-$ ionic potentials. Accessing these two potentials would require electron energies of ~7 eV and ~10 eV, respectively. For this reason, doubly excited high-Rydberg levels are expected to be absent in this E range and the doubly excited levels expected to drive DR must be of low-Rydberg or valence character. Thus, the observed high nitrogen Rydberg final states must be created in a later phase of the fragmentation process. This likely takes place at those internuclear distances where adiabatic potential curves below the $X\,^2\Pi$ ionic ground state have avoided crossings among each other. These avoided crossings, found for many states [10] not included in figure 1, indicate that their molecular orbital configurations are strongly coupled by configuration interaction among each other and with that of a doubly excited dissociating potential energy curve. Hence, during the variation of the internuclear distance in this region, the molecular state may lose its low-Rydberg or valence character and the ionic core is de-excited, while the outer electron is excited to high-Rydberg levels. As schematically indicated by the upper branch of path A, N* high-Rydberg levels of channel group I are populated. It should be noted that the Rydberg atoms pass through the first TSR dipole magnet downstream of the electron target at approximately the ion beam velocity and there experience a motional electric field amounting to ~110 kV cm^{-1} in the present work. Hence, atoms in states $n > n_{cut}$ are field ionized there and do not reach the detector. For the present results, we expect $n_{cut} \sim 10$ [26]. Figure 2 shows final Rydberg states up to $n = 10$.

Figure 2(b) shows data for $E = 6.2$ eV. At this energy, the increase of $P(d)$ at larger d indicates that a higher fraction of final population is found in lower excited levels of channel groups I or II. This could be caused by similar low-Rydberg or valence doubly excited states in the FC region as seen in figure 2(a) with the difference that the configuration change in the region of avoided crossings between high-Rydberg levels below the $X\,^2\Pi$ or a $^4\Sigma^-$ ionic curves is less efficient. The observed final channels indicate that the passage through the avoided crossing region in this case mostly leaves the molecule in low-Rydberg or valence excited states (lower branch of the schematic path A in figure 1).

Figure 2(b) also shows the development of a small structure at low d (~14 mm) indicating some contribution from final states H($n \sim 4, 5$) of channel group III. At $E = 7.1$ eV, shown in figure 2(c), this structure in $P(d)$ evolves into a marked peak whose maximum clearly indicates the presence of high H* Rydberg levels of channel group III. In fact, this energy lies in the range where high-Rydberg doubly excited neutral states attached to the shallow $2\,^2\Pi$ ionic potential curve can be present. These offer a direct fragmentation route to levels of exactly the observed property (path B in figure 1). Hence, we conclude that the characteristic peak occurring in $P(d)$ for a narrow range in energy around $E = 7.1$ eV is associated with electrons captured into high-Rydberg neutral states below the $2\,^2\Pi$ ionic curve and represents high-Rydberg atoms of hydrogen together with nitrogen fragment in the excited ^2D term of the ground configuration.

By the time we reach $E = 7.6$ eV, this peak nearly vanished, as can be seen in figure 2(d). This occurs without any significant discontinuity in the rate coefficient as a function of energy, leaving the final population mainly in lower excited levels of channel groups I or II, as was seen at lower E. This character of the final state population is retained up to higher E, smoothly developing into the shape seen in figure 2(e) at $E = 10.1$ eV, where high-Rydberg levels of channel group I (possibly also II) give a large contribution to the final states. At this energy, high-Rydberg doubly excited neutral states below the $2\,^4\Sigma^-$ ionic curve are present in the FC region and could directly dissociate in the observed range of E_k (path C in figure 1), likely resulting in N* Rydberg levels. This appears to be an important component of the transverse fragment distance distribution in figure 2(e).

In summary, we have measured transverse distance distributions for DR of the radical cation NH^+ over a range of electron collision energies above the bound states of the ion ($E = 4.2$–11.7 eV) and characterized the final states of the atomic products as a function of the collision energy. The production of high-Rydberg nitrogen atoms dominates at low ($E < 5$ eV) energies and appears to be important also at high energies ($E \sim 10$ eV). For energies above 6 eV, a significant fraction of the N and H fragments are produced with low levels of internal excitation. Moreover, in a small energy interval near 7 eV, hydrogen high-Rydberg products together with nitrogen in the first excited term are found. These results can be rationalized by considering the calculated $2\,^2\Pi$ and $2\,^4\Sigma^-$ excited potential energy curves of NH^+. The sharp energy dependence of the hydrogen Rydberg channel near 7 eV is compatible with the predicted shallow shape of the $2\,^2\Pi$ potential. This demonstrates the experimental capability to track the effect of the principal manifolds of doubly excited states contributing to DR and related neutral fragmentation, even though many final levels contribute and the structures are too complex to determine fragmentation branching ratios for them individually. For NH^+ DR at lower collision energies, transverse distance distributions can in fact be used to derive the energy-dependent branching ratios for individual final levels [25].

Acknowledgments

We thank the TSR accelerator group for efficient support during the experimental beamtime. BY was supported in part by Max Planck Society, CAS-MPS Doctoral Training program, the National Natural Science Foundation of China under grant nos 11179017 and 11275240, and National Basic Research Program of China (973 Program, no 2010CB832901). DS acknowledges support by the Weizmann Institute of Science through the Joseph Meyerhoff program.

ON and DWS were supported in part by the NSF Division of Astronomical Sciences Astronomy and Astrophysics Grants program and by the NASA Astronomy and Physics Research and Analysis Program. WDG acknowledges partial support by the COST Action CM0805: 'The Chemical Cosmos: Understanding Chemistry in Astronomical Environments'. Work is supported in part by the DFG Priority Program 1573 'Physics of the Interstellar Medium'.

References

[1] Hatano Y 1999 *Phys. Rep.* **313** 109
[2] Glass-Maujean M and Schmoranzer H 2005 *J. Phys. B: At. Mol. Opt. Phys.* **38** 1093
[3] Odagiri T *et al* 2011 *Phys. Rev.* A **84** 053401
[4] Azarm A *et al* 2011 *J. Phys. B: At. Mol. Opt. Phys.* **44** 085601
[5] Fischer A *et al* 2013 *Phys. Rev. Lett.* **110** 213002
[6] Larsson M and Orel A E 2008 *Dissociative Recombination of Molecular Ions* (Cambridge: Cambridge University Press)
[7] Wolf A, Buhr H and Novotný O 2011 *J. Phys.: Conf. Ser.* **300** 012008
[8] Buhr H *et al* 2010 *Phys. Rev.* A **81** 062702
[9] Amero J M and Vázquez G J 2005 *Int. J. Quantum Chem.* **101** 396
[10] Owono Owono L C *et al* 2007 *J. Chem. Phys.* **126** 244302
[11] Kawaguchi K and Amano T 1988 *J. Chem. Phys.* **88** 4584
[12] Grieser M *et al* 1993 *Nucl. Instrum. Methods* A **328** 160
[13] Poth H 1990 *Phys. Rep.* **196** 135
[14] Steck M *et al* 1990 *Nucl. Instrum. Methods* A **287** 324
[15] Sprenger F *et al* 2004 *Nucl. Instrum. Methods* A **532** 298
[16] Lestinsky M *et al* 2008 *Phys. Rev. Lett.* **100** 033001
[17] Krantz C *et al* 2009 *J. Phys.: Conf. Ser.* **192** 012025
[18] Orlov D A *et al* 2004 *Nucl. Instrum. Methods* A **532** 418
[19] Brzozowski J *et al* 1974 *Phys. Scr.* **10** 241
[20] Amitay Z, Zajfman D and Forck P 1994 *Phys. Rev.* A **50** 2304
[21] Novotný O *et al* 2013 in preparation
[22] Amitay Z *et al* 1996 *Phys. Rev.* A **54** 4032
[23] Kramida A, Ralchenko Y and Reader JNIST ASD Team 2012 NIST Atomic Spectra Database (version 5.0),(Gaithersburg: National Institute of Standards and Technology) (http://physics.nist.gov/asd)
[24] Ormonde S and Conneely M J 1971 *Phys. Rev.* A **4** 1432
[25] Yang B *et al* 2013 in preparation
[26] Schippers S *et al* 2001 *Astrophys. J.* **555** 1027